

Observations and analysis of small-scale magnetic flux ropes in the solar wind

Jinlei Zheng¹, Qiang Hu^{1,2}

¹Department of Space Science, University of Alabama in Huntsville, USA

²Center for Space Plasma and Aeronomics Research, University of Alabama in Huntsville, USA

E-mail: ¹jz0006@uah.edu

E-mail: ²qh0001@uah.edu

Abstract. The small-scale magnetic flux ropes (of duration ranging from a few minutes to a few hours) in the solar wind have the typical topology of winding field lines around a central axis, which is similar to the large-scale flux ropes, i.e., magnetic clouds. However, accumulating evidence suggests that their plasma characteristics, origin, formation mechanism and evolution are different from those of large-scale flux ropes. The small-scale flux ropes are intensively studied in recent years, since they affect particle transport and energization, and are considered as the potential source of local acceleration. The Grad-Shafranov reconstruction technique is a tool to reconstruct the two and a half dimensional field structure based on in-situ measurements captured by an observing platform moving past it. In this study, we reconstruct the flux rope structures in two events using the Grad-Shafranov reconstruction approach. In one event, a twin flux rope structure at 1 AU occurring on 2002 February 1 and two following single flux rope structures are identified behind an interplanetary shock. In the other event, we reconstruct the flux rope structures occurring on 1998 March 25 and 26 at 1 AU in the ambient solar wind. The associated energetic particle signatures and the possible origin of these flux rope structures are discussed.

1. Introduction

The magnetic flux ropes in the solar wind are an important type of transient and coherent structures in the inner heliosphere. Their formation, propagation and evolution shed light on the big picture of the space plasma dynamic processes. The magnetic field of a flux rope has the typical topology of winding field lines around a central axis with distributed currents. According to the scale size of the flux ropes in the solar wind, currently they are empirically classified into two categories: large-scale flux ropes and small-scale flux ropes. In addition to the difference in scale size, they also differ, sometimes, in terms of origination, formation mechanism, plasma profile and evolution process.

The large-scale flux ropes are also called magnetic clouds (MCs). The first magnetic cloud was identified by Burlaga et al. [1] in the solar wind between the heliocentric distances 1 AU and 2 AU. The spacecraft traversed a region with a radial dimension of 0.5 AU (0.25AU in radius), in which the measured magnetic field vectors rotated nearly parallel to a plane. In this region, the magnetic pressure dominated and the total pressure was higher than that of outside. Magnetic clouds are well defined observationally as a magnetic structure possessing these bulk properties



Content from this work may be used under the terms of the [Creative Commons Attribution 3.0 licence](#). Any further distribution of this work must maintain attribution to the author(s) and the title of the work, journal citation and DOI.

based on in-situ magnetic and plasma measurements: enhanced magnetic field strength, smooth rotation in magnetic field direction, and low proton temperature. They have been intensively studied in the past decades. It is widely accepted that the magnetic clouds have the following characteristics: (1) The topology of magnetic field is that of a helical structure, in which the field lines are winding around a central axis, forming the helix shape elongated along the axial dimension. As a spacecraft passes through the helical field lines of a flux rope, the in-situ data of magnetic field vectors show a smooth and continuous rotation. (2) The magnetic field in a magnetic cloud is stronger than the surrounding solar wind, and the magnetic pressure usually dominates. (3) The proton temperature is depressed within the magnetic cloud, resulting in ultra-low proton β value, the ratio between the proton plasma and magnetic pressure. Besides these key properties mentioned above, magnetic clouds have a typical radial scale size reaching a few tenths of an AU at 1 AU [2]. A limited number of studies also examined their radial evolution between 0.3 and 4.2 AU [3].

Observational evidence suggested that the magnetic clouds have a close relation to the coronal mass ejections (CMEs) [4, 5, 6, 7, 8]. The CMEs interact with ambient solar wind when they propagate into the heliosphere. Because the CMEs generally move faster than the ambient solar wind, they form the interplanetary coronal mass ejections (ICMEs), often driving a shock wave. At least a portion of ICMEs has the properties of magnetic clouds as crossed by a single spacecraft [9]. The fraction of MCs among ICMEs has a solar cycle phase dependence [10]. From the studies of 56 magnetic clouds at 0.7AU during 1979-1988, Mulligan and Russell [11] showed that the leading magnetic field in magnetic clouds was controlled by the solar global field. The studies by Lynch et al. [12] suggested that the net accumulative helicity of most magnetic clouds appeared to be modulated by solar activity cycle. The radial scale size of magnetic clouds expands as they move outward from the sun [1, 13, 14, 5, 15, 16]. Besides the radial expansion, a significant poloidal motion was also found in some magnetic clouds [16]. Magnetic flux ropes are also found in the Earth's magnetotail [17] and in other planetary environment. Some non-solar source magnetic flux ropes appear to be created by magnetic reconnection in local plasma environment, such as those by reconnection across the plasma sheet in magnetotail. Some small-scale flux ropes in the solar wind may share the same generation mechanism.

Past research usually employs a cylindrically symmetric, constant-alpha, linear force-free magnetic field model to fit the one-dimensional spacecraft data across a magnetic cloud [18, 19]. A simple solution of such a model was found by [20], in which the axial and transverse components are proportional to the zeroth-order and first-order Bessel functions of the first kind, respectively. Other similar 1D models also exist. However, these models are limited to a pre-defined 1D cross-section geometry and force-free condition. Alternatively, Hu and Sonnerup [21, 22] applied the Grad-Shafranov(GS) reconstruction technique [23, 24] to the in situ data collected when the spacecraft crosses the flux rope structures. In the GS reconstruction, axial symmetric and force-free assumptions are abandoned. The reconstruction results showed the obvious distortion from the axial symmetric geometry. The multiple, non-symmetric flux rope structures were reconstructed by Hu et al. [25] using the GS reconstruction technique. These structures had the double or triple flux rope configurations, in which one flux rope was located immediately next to the other. The magnetic X point/line between adjacent flux ropes implied that they may be relics of the end product of a dynamic evolution process due to magnetic reconnection.

The small-scale flux ropes have the magnetic field geometry similar to large-scale flux ropes, i.e. MCs. However, they have much smaller scale sizes ranging from ~ 0.001 to 0.01 AU, and the identification of small-scale flux ropes is less definitive. Unlike MCs which have a clear

association with CMEs, originating from solar corona, the origin of small-scale flux ropes is still debatable. Moldwin et al. [26] reported a non-CME flux rope at 5 AU. The scale size of this flux rope is about 0.05 AU, and the plasma profile is different from that of magnetic clouds. They interpreted this flux rope as a result of multiple magnetic reconnection at the heliospheric current sheet (HCS). The concept of small-scale flux ropes was first introduced by Moldwin et al. [27]. They observed some flux ropes with smaller sizes compared with MCs at 1 AU, while the former had durations of tens of minutes as opposed to a dozen hours to days of MCs. They suggested that these small-scale flux ropes were products of magnetic reconnection in the local solar wind, instead of in the solar corona.

In recent years, small-scale flux ropes have attracted interest of researchers on its different characteristics compared with MCs. Feng et al. [28] identified 144 magnetic flux ropes with radial scale sizes from about 0.004 to 0.6 AU (including both large and small scale flux ropes). Based on the similarity of their energy distributions to solar flares, they suggested that the small-scale and intermediate-scale flux ropes were the interplanetary manifestations of some small CME events. Cartwright and Moldwin [29] identified 68 flux ropes with strong core field using WIND magnetic field data. They excluded the possible mixture of Alfvén waves in the identification. The duration ranged from 39 minutes to 12.2 hours. The comparison showed that these two kinds of flux ropes differed in terms of expansion, whether or not in force-balance, the strengths of core fields, and the association with forward shocks, which implied that they may have different origins. Feng et al. [30] surveyed 125 small-scale and intermediate-scale flux ropes. They suggested that the small-scale and intermediate-scale flux ropes originated from solar eruptions, similar to MCs, since they had similar characteristics. Cartwright et al. [31] did a comprehensive survey of small-scale flux ropes located between 0.3 and 5.5 AU. They found that the occurrence of small-scale flux ropes had a solar cycle dependency, which implies that they may originated from the sun. However, they also found that the lack of depressing proton temperature and the location being near the sector boundary crossings implied that they may be created locally due to magnetic reconnection across the heliospheric current sheet. More recently, Feng et al. [32] examined the counterstreaming suprathermal electron (CSE) signatures of 106 small-scale flux ropes measured by WIND from 1995-2005. They found that the CSE appeared in most small-scale flux ropes located far from the heliospheric current sheets (HCSs), while the CSE appeared in only half of the small-scale flux ropes located near the heliospheric current sheets. A limited number of studies also looked at the corresponding elemental composition and charge state signatures within small-scale flux rope intervals [32]. By using hourly data, those authors found from a subset of small-scale flux rope events identified between 1995 and 2007 that these structures share some common features with MCs. They provided supporting evidence for the origin of small-scale flux ropes from solar corona.

As discussed above, our understanding on small-scale flux ropes is far from comprehensive. Their formation mechanism and origination are still under debate. And the hypotheses of evolution and propagation process are based on insufficient database. The coverage of the latest database is before 2007. The energetic particle profiles related to small-scale flux ropes are less studied. Theoretical studies suggested that small-scale flux rope activities such as contracting, merging (reconnection) can lead to particle acceleration [33, 34]. The observational evidence of the existence of such flux ropes, supported by sound analysis via the GS method, remains to be discovered. The most used model of small-scale flux rope is static constant-alpha force-free cylindrically symmetric field model [18, 19]. This model restricts the fitted small-scale flux ropes to a simple geometry of circular cross section, omitting plasma pressure gradient, which is not consistent with observations. The Grad-Shafranov reconstruction model [21, 22, 25] is able to recover the non-symmetric geometry of the small-scale flux rope in a more general non-force

free configuration. So far, it has not been systematically applied to examine the magnetic field configuration of small-scale flux ropes in the solar wind. Furthermore, Sonnerup et al. [35] have developed a basic approach for 2-D time-stationary, ideal, and compressible MHD reconstruction technique that can account for significant remaining plasma flow within the structure. This technique can be implemented in small-scale flux rope reconstructions to recover both the magnetic field and plasma flow structures in dynamic equilibrium.

In this study, we apply the GS reconstruction method to reconstruct a handful of small-scale flux rope structures under different background solar wind conditions. One set of cases is found behind an interplanetary traveling shock and the other set of cases is in the ambient, ordinary solar wind, not associated with an apparent solar source, such as a CME, or a high-speed stream.

2. Grad-Shafranov Reconstruction Technique

The Grad-Shafranov (GS) reconstruction technique is a tool for the reconstruction of $2\frac{1}{2}$ -D coherent magnetic field structure from data collected as the structure moves past an observing platform. It was first developed and applied to magnetopause crossings [23, 36, 37]. Hu et al. further developed this technique and applied it to magnetic flux ropes in the solar wind [21, 22, 25]. The GS reconstruction technique is based on the more general non-force-free assumption, and is able to recover the distortion of a flux rope from axial symmetric geometry.

In GS reconstruction technique, the magnetohydrostatic equilibrium assumption is adopted to describe the magnetic field structures. Such a configuration is in static force balance between the plasma pressure gradient and the Lorentz force,

$$\nabla p = \mathbf{j} \times \mathbf{B}. \quad (1)$$

There are two other conditions satisfied by the magnetic field which are $\nabla \cdot \mathbf{B} = 0$ and $\nabla \times \mathbf{B} = \mu_0 \mathbf{j}$. In a cylindrical flux rope, the variation along axial direction is much more gradual than that in the transverse direction. So we can assume that the magnetic field and plasma equilibrium has the translation symmetry along the axial direction (the z axis), which is perpendicular to the transverse plane (the cross-sectional $x - y$ plane). With this assumption, the derivative with respect to z is zero ($\partial/\partial z = 0$). The reconstruction is carried out in a co-moving frame of reference, in which the electric field \mathbf{E}' vanishes. Usually the deHoffmann-Teller (HT) frame is used [38, 39, 40]. With $\mathbf{E}' = 0$, we have $\nabla \times \mathbf{E}' = -\frac{\partial \mathbf{B}}{\partial t'} = 0$, indicating a stationary magnetic field structure. Making use of the magnetic flux function $A(x, y)$ such that the magnetic field vector is

$$\mathbf{B} = [\partial A / \partial y, -\partial A / \partial x, B_z(A)], \quad (2)$$

one can reduce the Equation (1) to a scalar equation

$$\frac{\partial^2 A}{\partial x^2} + \frac{\partial^2 A}{\partial y^2} = -\mu_0 \frac{d}{dA} (p + B_z^2 / 2\mu_0) = -\mu_0 \frac{dP_t}{dA}. \quad (3)$$

The above equation (3) is the so-called Grad-Shafranov(GS) equation. By solving it numerically [36], the reconstructed map of $A(x, y)$ is obtained. Then the magnetic field \mathbf{B} is acquired by taking derivatives of $A(x, y)$ and a functional fitting, $B_z(A)$.

In practice, we follow the basic reconstruction steps described in the paper by Hu and Sonnerup [22]. The first step is to find a co-moving frame of reference, which is usually the deHoffmann-Teller (HT) frame [38, 39, 40]. This is achieved by minimizing the residual electric

field of a frame moving with an unknown velocity. In the ideal case, the residual electric field can be transformed to zero. Then the minimum-variance analysis is applied to find three eigenvalues (the minimum, intermediate, and maximum covariances) and the corresponding eigenvectors. We take the direction along the intermediate eigenvector as the initial trial z axis. A trial-and-error process is carried out to find the optimal z axis orientation, based on the requirement of $P_t(x, 0) \sim A(x, 0)$ being single-valued. The spacecraft data are projected onto the local reconstruction coordinate (x, y, z) , in which the projected spacecraft path is along the positive x direction on the plane perpendicular to z , and the y axis completes the right-handed orthogonal coordinate system. Next we integrate the measured $B_y(x, 0)$ to obtain the value $A(x, 0)$. By fitting the data pairs $P_t(x, 0)$ and $A(x, 0)$, we obtain an analytic function for the transverse pressure $P_t(A)$. Using the known function $P_t(A)$ and initial values given by spacecraft measurements along $y = 0$, we solve the GS equation [36] to obtain the solution of the flux function $A(x, y)$ in a rectangular domain on the cross section perpendicular to z , which fully characterizes the $2\frac{1}{2}$ -D magnetic field configuration of the flux rope.

3. Case Studies

In this section, we present two sets of case studies of small-scale magnetic flux ropes selected from WIND spacecraft data. Cases 1, 2 and 3 belong to an event on Feb. 1st, 2002, all of which are behind an interplanetary shock. Case 4 and 5 are on Mar. 25th, 1998, both of which are in ambient solar wind with no apparent and direct solar source correspondence. Below we present relevant and detailed observations and GS reconstruction results of these cases.

3.1. Flux ropes behind an interplanetary shock

Figure 1 shows that three small-scale flux ropes were identified behind an interplanetary shock. The shock interface was observed on 2002 Jan. 31, 21:38 UT. It is denoted by a vertical dashed line. We can see that the magnetic field magnitude jumps at the shock interface. All magnetic field components change accordingly. Three small-scale flux rope intervals were marked based on mainly magnetic field measurements and the GS reconstruction results to be presented. The magnetic field magnitude kept at a high level (about 12 nT) downstream of the shock, together with elevated solar wind flow speed. The second panel shows that the solar wind speed was enhanced from about 280 km/s to about 360 km/s downstream across the shock interface. These were not typically high speed. The third panel shows that the proton density (in blue color) and the alpha/proton number density ratio changed drastically in the downstream of the shock. It is generally believed that higher alpha/proton ratio implies a coronal source of the plasma. In the last panel, we can see that the proton temperature increased in case 1 and case 2. In case 3, the proton temperature decreased but was still above that in ambient solar wind. This temperature characteristic is different from that of a magnetic cloud, in which the proton temperature is depressed. The average plasma beta values during the time intervals of case 1 and case 3 were 0.09 and 0.14, respectively. These values were close to the typical plasma beta value in MCs ($\lesssim 0.1$). The average plasma beta value during the time interval of case 2 was 0.33, which was above that of MCs.

We also examined the energetic particle profile associated with these flux rope structures. Figure 2 shows the energetic ion dispersion observed by ACE ULEIS instrument. The date range of the top panel is from 2002, Jan. 27 to the end of Jan. 30, which is several days before the flux rope structures were observed. Three flux rope intervals are shown in the bottom panel, which are denoted by the shaded regions in sequence. The dots in this figure represent the energetic ion events, and the colors of dots denote the counts in each energy bin. The inverse slope of each slanted line denotes a nominal length ~ 1.2 AU traversed by a particle. If the bulk of energetic

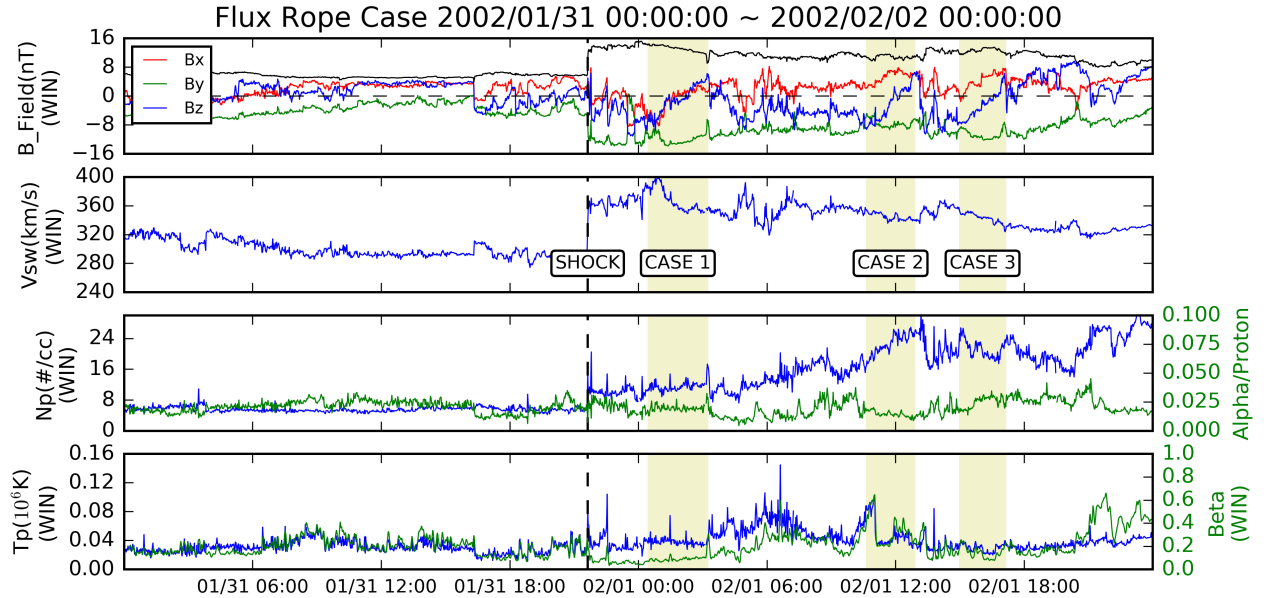
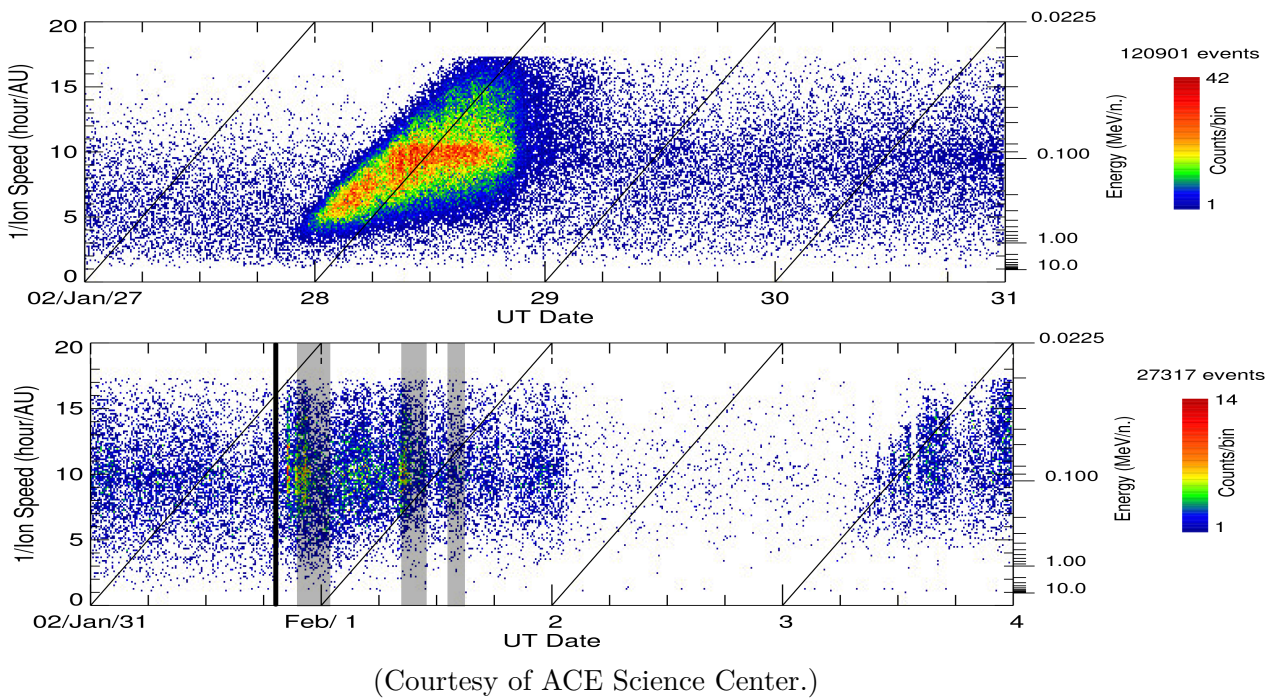


Figure 1. WIND spacecraft data from 2002 Jan. 31, 00:00 UT to 2002 Feb. 2, 00:00 UT. This time interval contains one interplanetary shock and three flux rope structures. The first panel is the magnetic field data from MFI. The black solid line denotes the total magnetic field magnitude. The second panel is the solar wind bulk speed from SWE. In the third panel, the proton number density is shown in blue line and the alpha/proton number density ratio is shown in green line. These two sets of data are from SWE. The fourth panel are the proton temperature (in blue line) and plasma $\beta = N_p k T_p / (B^2 / 2\mu_0)$ (in green line). The contribution of electrons to plasma β was not included, because the electron temperature was not available. The shock is denoted by a vertical black dashed line. The time of this shock is 2002 Jan. 31, 21:38 UT. The shaded regions represent three small-scale flux ropes, which are labeled by CASE 1, CASE 2 and CASE 3, respectively.

particles was created at the same time and location near the Sun, and if they travel to 1 AU nearly scatter-free, the representing dots will align along the line. The triangular distribution of the enhanced ion population between Jan. 28 and Jan. 29 probably implies significant scattering and other effects on the energetic ions propagating en route from the source to 1 AU within one day. After checking the solar activities, we found there was a halo CME occurred at 2002 Jan. 27, 12:30:05 UT with a speed of 1135 km/s. This was probably the source of those energetic particles. In the bottom panel of Figure 2, the shaded regions represent the case 1, case 2, and case 3 in sequence. The vertical thick black line denotes the location of shock interface. The particle counts were enhanced immediately behind the shock interface, with no clear pattern, which means these particles were created locally, probably energized by the shock. Furthermore, behind the shock, there were three obvious counts enhancement regions. They appear to coincide, partially, with the time intervals of the first two flux ropes identified. Next we are going to present the reconstruction results of case 1, case 2, and case 3 in details.

3.1.1. CASE 1: WIND 2002/2/1 0:25 - 3:15 UT The reconstruction result of case 1 is shown in Figure 3(a). We can see a twin flux rope structure from Figure 3(a). This kind of structure



(Courtesy of ACE Science Center.)

Figure 2. The energetic particles profile for Case 1, 2 and 3, which are denoted by three shaded regions in sequence. The data are obtained from ACE ULEIS instrument. The energy range is from 0.0225 MeV to 10 MeV, and the mass range is from 10 to 70 AMU, which includes the Fe, Ca, S, Si, Mg, Ne, O, N, and C elements. The color denotes counts/bin. The left Y axis is the inverse ion speed represented by hour/AU, and the right Y axis is the corresponding energy in MeV/n.

was reconstructed and studied earlier by Hu et al. [25], but for large-scale MCs. The core fields of these two adjacent flux ropes are about 13 nT. The time duration of the entire event was 2 hours and 50 minutes. The flux rope on the left had a scale size of about 0.0075 AU, and the right one had a scale size of about 0.01 AU. From the white arrow we can see that both of them had the right chirality. An X point may be formed by magnetic reconnection yielding this geometry. Figure 3(b) is the fitting curve of $P_t(A)$, which is the transverse plasma pressure, the sum of plasma and axial magnetic pressure. According to the GS reconstruction theory, $P_t(A)$ must be a single valued function of magnetic flux function A . The R_f in the graph is the fitting residue. It is the normalized deviation of the measured data from the fitted curve, which was defined in the paper by Hu et al. [25]. In this case, the residue is 0.15. We consider the fitting with a residue below 0.3 as a reliable fitting. The last panel of Figure 1 shows that the proton temperature was not depressed during the time interval of case 1, which is different from that of MCs.

3.1.2. CASE 2: WIND 2002/2/1 10:36 - 12:55 UT The reconstruction result of case 2 is shown in Figure 4. The time duration was 2 hours and 19 minutes, and the scale size was about 0.01 AU. The core field of this flux rope was about 11nT. The chirality was right-handed, which is the same as that in case 1. This reconstruction has a fitting residue of 0.08 (see Figure 4(b)), which is a very small value, indicating a trustworthy reconstruction. From the third panel of

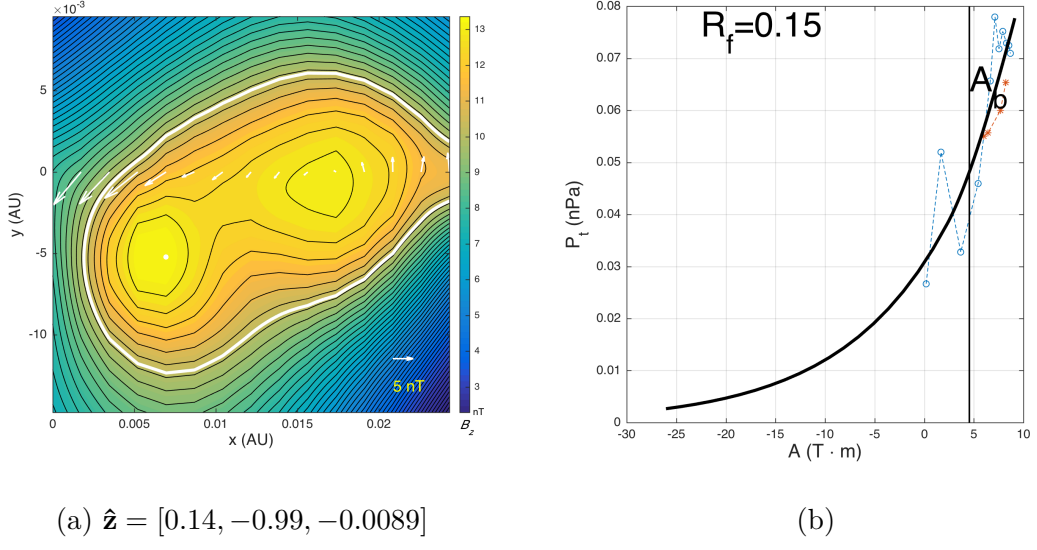


Figure 3. GS reconstruction result for Case 1 (2002 Feb. 1, 0:25 - 3:15 UT). (a) The cross-section magnetic field configuration of the flux rope. The unit vector \hat{z} represents the z axis orientation of the flux rope in GSE coordinate. The filled color contour represents the axial magnetic field B_z and the overlapped black contour lines represent the transverse magnetic field. The white dot in the center is the location of maximum axial field B_{zmax} . The white arrows along $y = 0$ are measured transverse magnetic field vectors along the spacecraft path. The white contour line encloses the region $A > A_b$, as denoted in (b). The reconstruction map within this line is reconstructed by double-folded satellite data, and the region beyond this line is reconstructed based on the extrapolated data. (b) The fitting curve (bold solid line) of $P_t(A)$ for Case 1. The fitting is based on the data points denoted by blue circles and red stars, where the circles represent the data along the first half of the spacecraft path and the stars represent those of the second half. The thin vertical solid line denoted by A_b marks the boundary corresponding to the white enclosure line in (a).

Figure 1, we can see that the proton number density was much higher than that of case 1. But the alpha/proton ratio was similar to that of case 1, indicating that the number density of both protons and alpha particles enhanced. The proton temperature was enhanced at the beginning of case 2, then dropped to the same level as that of case 1.

3.1.3. CASE 3: WIND 2002/2/1 14:57 - 17:03 UT The reconstruction result of case 3 is shown in Figure 5. Figure 5(b) shows the fitting curve of function $P_t(A)$ with a low fitting residue 0.07. From Figure 5(a), we can see that the satellite crossed the cross-section of this flux rope near the central axis. The duration of this flux rope was 2 hour and 6 minutes, and its scale size was about 0.015 AU. It had the same right-handed chirality as that of case 1 and case 2. Figure 1 shows that case 3 also had the high proton number density. The average plasma beta value was 0.14, which is close to the typical value in MCs.

From the three cases above, we find that the multiple small-scale flux ropes exist in downstream of a shock. None of them showed the depressed proton temperature. Two cases (case 1 and case 3) had the similar plasma beta values to that of MCs, and one case (case 2) had the

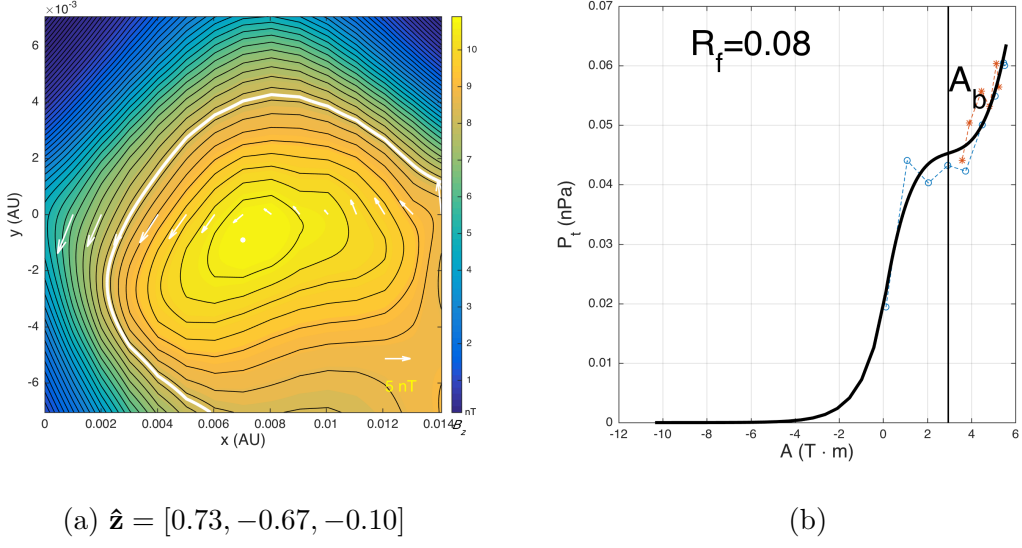


Figure 4. GS reconstruction result for Case 2 (2002 Feb. 1, 10:36 - 12:55 UT). The format is the same as that in Figure 3.

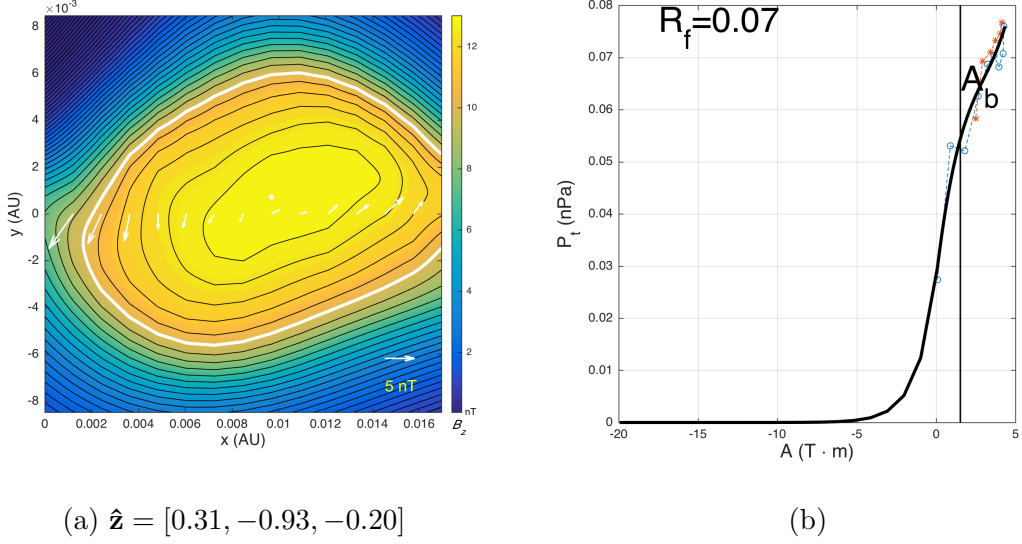


Figure 5. Flux rope reconstruction for Case 3 (2002 Feb. 1, 14:57 - 17:03 UT). The format is the same as that in Figure 3.

higher plasma beta value than that of MCs. There were energetic particle flux enhancements associated with them (see second panel of Figure 2), at least partially. Such associations between particle energization and the small-scale flux rope structures were examined by Trenchi et al.[41] and a mechanism involving both diffusive shock acceleration and the magnetic flux ropes was developed by Zank et al.[42]. A Halo CME occurred at 2002 Jan. 27, 12:30:05 UT was a possible source to drive the shock and generate the trailing complex structure behind the shock. However, given the different plasma profiles from typical MCs, these small-scale flux ropes may not be generated on the Sun by the CME. They may be produced by the shock, or some other

processes in the inner heliosphere. The same chirality of the three flux ropes may hint at the same process or the same environment in which they were generated.

3.2. Flux ropes in ambient solar wind

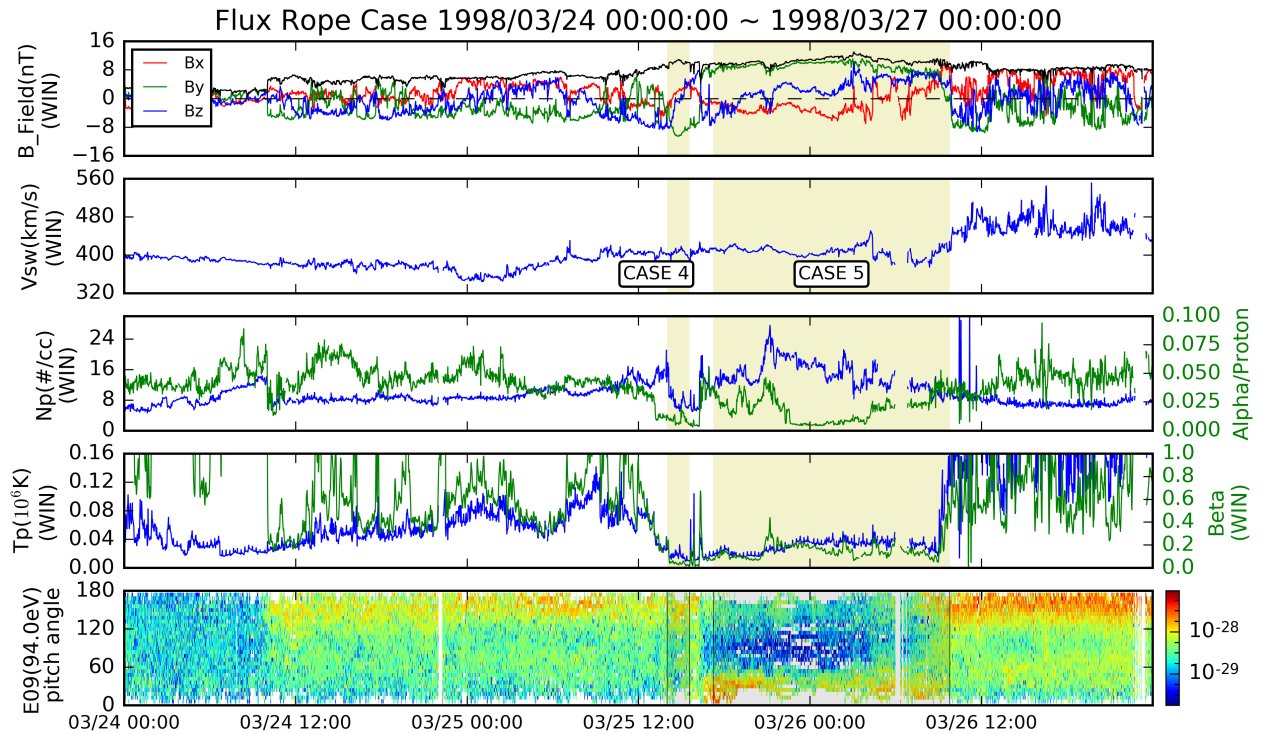


Figure 6. Time series data from 1998 Mar. 24, 00:00 UT to 1998 Mar. 27, 00:00 UT. This time interval contains two flux rope structures. The format of the first four panels are the same as Figure 1. The bottom panel is the suprathermal electron pitch angle spectrogram with the energy of 94.0 eV, obtained by the SWE instrument on WIND.

Figure 6 shows the time series which covers the case 4 and case 5. In this event, the suprathermal electron pitch angle data are available and are shown in the bottom panel. The shaded regions represent the time intervals of case 4 and case 5, respectively. During the interval of case 4, both B_x and B_z components rotated smoothly from negative to positive, while B_y component changed from about -8 nT to 4 nT. The total magnetic field magnitude was about 10 nT across the interval of case 4. During the interval of case 5, there were fluctuations overlapped on the rotation trend, especially in the latter half. The large trend shows that the B_z component rotated from negative to positive, and the B_y component remained uni-directional. The solar wind speed(second panel) was about 400 km/s, which is a bit higher than that of the first three cases. The third panel shows the proton number density (in blue) and the alpha/proton ratio (in green). The proton density was depressed in case 4 and then enhanced in case 5. The fourth panel shows that the proton temperature across case 4 and case 5 was depressed. The average plasma beta (proton temperature only) value in case 4 was about 0.05, which is a very low value, indicating that the magnetic pressure dominates in pressure balance. This value in case 5 was 0.15, indicating a relatively enhanced plasma pressure. From the bottom panel we can see that

the flux of suprathermal electrons with large pitch angle(120° - 180°) was enhanced in case 4, while the flux of suprathermal electrons with small pitch angle(0° - 60°) was enhanced in case 5. The gap between case 4 and case 5 is also noteworthy. In this gap, all three magnetic field components changed the sign, indicating a direction reversal of magnetic field. We will discuss this in more details below.

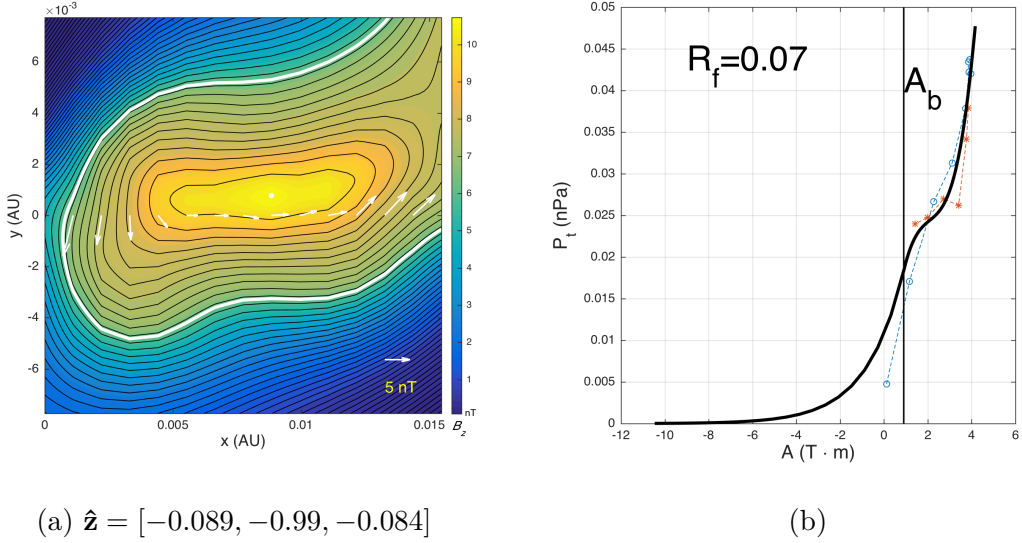


Figure 7. GS reconstruction result for Case 4 (1998 Mar. 25, 14:03 - 15:39 UT). The format is the same as that in Figure 3.

3.2.1. CASE 4: WIND 1998/3/25 14:03 - 15:39 UT Figure 7(a) shows the GS reconstruction of the small-scale flux rope in case 4. Figure 7(b) shows that the fitting residue is 0.07. This flux rope had a time duration of 1 hour and 36 minutes, and a scale size of 0.01 AU. It had the right-handed chirality. The core field is about 11 nT. According to the bottom panel in Figure 6, the suprathermal electrons with large pitch angles (120° - 180°) was enhanced, which implied the electrons were moving anti-parallel to the magnetic field lines. We will compare it with case 5 below.

3.2.2. CASE 5: WIND 1998/3/25 17:14 - 1998/3/26 09:47 UT Compared with the first four small-scale flux ropes, case 5 had a bigger scale size. Figure 8(a) shows that its scale size was about 0.1 AU, which is ten times as large as the first four flux ropes. This size is approaching the lower limit of the MC scale size. Therefore, we can take it as an intermediate-scale flux rope. The time duration was about 16 hours and 33 minutes, although arguably the interval can be shortened, for example, by excluding the later part showing enhanced fluctuations in magnetic field. Its core field was about 12 nT, which is stronger than that of case 4. Figure 8(b) shows that the fitting residue was 0.09, which is a relatively good fitting. From the fourth panel in Figure 6, we can see that the proton temperature(in blue) across the entire flux rope was depressed. Taking into account the plasma beta value (0.15 on average), this profile is similar to that of MC. The most interesting phenomenon is the suprathermal electrons pitch angle spectrogram(see the bottom panel in Figure 6). At the start of the time interval of case 5, the pitch angle of most suprathermal electrons suddenly changed from 120° - 180° to 0° - 60° , and

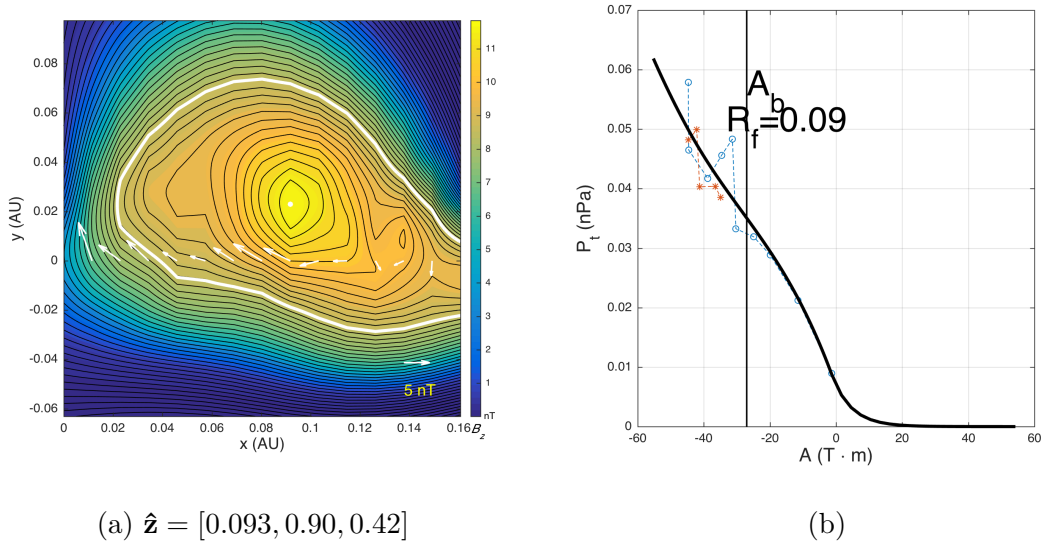


Figure 8. Flux rope reconstruction for Case 5 (1998 Mar. 25, 17:14 - Mar. 26, 09:47 UT). The format is the same as that in Figure 3.

in the end of this interval, the pitch angle of most suprathermal electrons changed back. This flux rope had the left-handed chirality, which is opposite to that of case 4. After checking the z axis directions of these two flux ropes, we found that they had opposite orientation. In case 4, the unit vector of z axis is $[-0.089, -0.99, -0.084]$ in GSE, while in case 5, the unit vector of z axis is $[0.093, 0.90, 0.42]$ in GSE. The angle between them is about 160° , which means that they are approximately anti-parallel. The hypothesis we proposed in Section 3.2 is supported by this result. Now we are ready to explain the behavior of the suprathermal electrons. Actually, the moving direction of these electrons had not changed. Because the flux rope in case 4 flipped the axial direction compared to the flux rope in case 5, the electron pitch angles changed from 120° - 180° to 0° - 60° when the electrons were streaming outward along field lines. The flipping is supported by the fact that in the gap between case 4 and case 5, all of the three components of magnetic field flipped the direction (see the first panel in Figure 6). Because of the anti-parallel directions of the z axes, though case 4 and case 5 have different chirality, in fact the transverse field lines in their adjacent region are anti-parallel. This geometry is able to produce magnetic field line reconnection resulting in a possible configuration of magnetic separatrix. Another interesting fact is, the pitch angle spectrogram of the suprathermal electrons remains unchanged across the flux rope interval in case 5. The bottom panel of Figure 6 also shows that the electrons with pitch angle near 90° were depleted in the flux rope structure.

4. Summary and Discussion

In summary, we have reconstructed four small-scale magnetic flux ropes and one intermediate-scale magnetic flux rope in the solar wind, using the Grad-Shafranov reconstruction technique. Three of these flux ropes were downstream an interplanetary traveling shock, and two of them were in the ambient solar wind. Table 1 summarizes the key parameters obtained for these cases examined in this paper. All of them have relatively strong core magnetic field (see last column in Table 1), and are located in slow solar wind (the average solar wind speed, $\approx V_{HT}$, $\lesssim 400$ km/s). Our study suggests that (1) there exists multiple small-scale magnetic flux ropes behind an interplanetary traveling shock. Additional observations showed their possible associations

Table 1. Summary of five magnetic flux ropes.

Case No.	Duration ^(a)	$(\delta, \phi)^{(b)}$	$\langle \beta \rangle^{(c)}$	$V_{HT}^{(d)}$	$\Phi_t^{(e)}$	$\Phi_p^{(f)}$	$\tau^{(g)}$	$B_{zmax}^{(h)}$
1	2.83	(82°, 181°)	0.09	347	7.2E10	6.8E11	9	13
2	2.32	(43°, 189°)	0.33	356	2.4E10	3.9E11	16	11
3	2.10	(72°, 192°)	0.14	350	3.5E10	4.2E11	12	13
4	1.60	(95°, 185°)	0.05	404	2.4E10	4.9E11	20	11
5	16.55	(85°, 25°)	0.15	403	2.1E12	4.2E12	2	12

(a) The time duration of a flux rope (hours).

(b) The δ is the polar angle of the axial direction of a flux rope with respect to solar radial direction, and the ϕ is the azimuthal angle of the axial direction of a flux rope, projected onto the plane of sky, with respect to the Z axis in GSE coordinate.

(c) The average plasma beta value (no electron temperature contribution).

(d) The speed of the deHoffmann-Teller(HT) frame (km/s).

(e) The total axial magnetic flux within the boundary $A = A_b$ of a flux rope (Wb).

(f) The poloidal magnetic flux per 1 AU of a magnetic flux rope (Wb).

(g) The ratio of Φ_p to Φ_t , indicative of average magnetic field-line twist.

(h) The maximum axial magnetic field of a flux rope (nT).

with the energetic particle enhancement. A combined and detailed analysis of all available in-situ observations within certain theoretical framework is needed to further elucidate such associations and the roles of magnetic flux ropes in particle transport and energization. (2) The small-scale magnetic flux ropes occurred in different regions tend to have different characteristics. For example, in the region downstream an interplanetary traveling shock, the small-scale magnetic flux ropes didn't show the depressed proton temperature. The number density ratio of alpha to proton kept at a relatively steady ratio. In the region of ambient solar wind, our two cases showed the obviously depressed proton temperature, which is a typical characteristic of MCs. These differences indicate that they may have different origins and formation mechanisms, and also imply their different capabilities to energize particles.

Acknowledgments

We would like to thank NASA's Space Physics Data Facility for the WIND spacecraft data, and ACE Science Center for ACE data and the energetic ion plots. We acknowledge NASA grants NNX12AH50G, NNX14AF41G and NRL contract N00173-14-1-G006 (NNH13ZDA001N) for support.

References

- [1] Burlaga L, Sittler E, Mariani F and Schwenn R 1981 *Journal of Geophysical Research: Space Physics* **86** 6673–6684 ISSN 2156-2202 URL <http://dx.doi.org/10.1029/JA086iA08p06673>
- [2] Lepping R P, Jones J A and Burlaga L F 1990 *Journal of Geophysical Research: Space Physics* **95** 11957–11965 ISSN 2156-2202 URL <http://dx.doi.org/10.1029/JA095iA08p11957>
- [3] Bothmer V and Rust D 1997 *The Field Configuration of Magnetic Clouds and the Solar Cycle* (American Geophysical Union) pp 139–146 ISBN 9781118664377 URL <http://dx.doi.org/10.1029/GM099p0139>
- [4] Smith C W and Phillips J L 1997 *Journal of Geophysical Research: Space Physics* **102** 249–261 ISSN 2156-2202 URL <http://dx.doi.org/10.1029/96JA02678>
- [5] Bothmer V and Schwenn R 1998 *Annales Geophysicae* **16** 1–24 URL <http://www.ann-geophys.net/16/1/1998/>

- [6] Wilson A (ed) 2003 *Proc. Sources of magnetic helicity over the solar cycle*
- [7] Leamon R J, Canfield R C, Jones S L, Lambkin K, Lundberg B J and Pevtsov A A 2004 *Journal of Geophysical Research: Space Physics* **109** ISSN 2156-2202 a05106 URL <http://dx.doi.org/10.1029/2003JA010324>
- [8] Innes D E, Lagg A and Solanki S K (eds) 2003 *Proc. Quantitative Link Between Solar Ejecta and Interplanetary Magnetic Clouds: Magnetic Helicity*
- [9] Pizzo V J, Holzer T E and Sime D G (eds) 2003 *Proc. The origin and propagation of coronal mass ejections*
- [10] Richardson I G and Cane H V 2004 *Geophysical Research Letters* **31** ISSN 1944-8007 l18804 URL <http://dx.doi.org/10.1029/2004GL020958>
- [11] Mulligan T, Russell C T and Luhmann J G 1998 *Geophysical Research Letters* **25** 2959–2962 ISSN 1944-8007 URL <http://dx.doi.org/10.1029/98GL01302>
- [12] Lynch B J, Gruesbeck J R, Zurbuchen T H and Antiochos S K 2005 *Journal of Geophysical Research: Space Physics* **110** ISSN 2156-2202 a08107 URL <http://dx.doi.org/10.1029/2005JA011137>
- [13] Burlaga L F and Behannon K W 1982 *Solar Physics* **81** 181–192 URL <http://dx.doi.org/10.1007/BF00151989>
- [14] Klein L W and Burlaga L F 1982 *Journal of Geophysical Research: Space Physics* **87** 613–624 ISSN 2156-2202 URL <http://dx.doi.org/10.1029/JA087iA02p00613>
- [15] Lepping R P, Berdichevsky D B, Wu C C, Szabo A, Narock T, Mariani F, Lazarus A J and Quivers A J 2006 *Annales Geophysicae* **24** 215–245
- [16] Wang Y, Zhou Z, Shen C, Liu R and Wang S 2015 *Journal of Geophysical Research: Space Physics* **120** 1543–1565 ISSN 2169-9402 2014JA020494 URL <http://dx.doi.org/10.1002/2014JA020494>
- [17] Moldwin M B and Hughes W J 1992 *Journal of Geophysical Research: Space Physics* **97** 19259–19282 ISSN 2156-2202 URL <http://dx.doi.org/10.1029/92JA01598>
- [18] Neugebauer B (ed) 1983 *Proc. On the field configuration in magnetic clouds* (NASA Conf. Publ., NASA CP-2280)
- [19] Burlaga L F 1988 *Journal of Geophysical Research: Space Physics* **93** 7217–7224 ISSN 2156-2202 URL <http://dx.doi.org/10.1029/JA093iA07p07217>
- [20] Lundquist S 1950 *Ark. Fys.* **2** 361–365
- [21] Hu Q and Sonnerup B U 2001 *Geophysical Research Letters* **28** 467–470 ISSN 1944-8007 URL <http://dx.doi.org/10.1029/2000GL012232>
- [22] Hu Q and Sonnerup B U O 2002 *Journal of Geophysical Research: Space Physics* **107** SSH 10–1–SSH 10–15 ISSN 2156-2202 URL <http://dx.doi.org/10.1029/2001JA000293>
- [23] Sonnerup B U O and Guo M 1996 *Geophysical Research Letters* **23** 3679–3682 ISSN 1944-8007 URL <http://dx.doi.org/10.1029/96GL03573>
- [24] Sonnerup B U O, Hasegawa H, Teh W L and Hau L N 2006 *Journal of Geophysical Research: Space Physics* **111** ISSN 2156-2202 a09204 URL <http://dx.doi.org/10.1029/2006JA011717>
- [25] Hu Q, Smith C W, Ness N F and Skoug R M 2004 *Journal of Geophysical Research: Space Physics* **109** ISSN 2156-2202 a03102 URL <http://dx.doi.org/10.1029/2003JA010101>
- [26] Moldwin M B, Phillips J L, Gosling J T, Scime E E, McComas D J, Bame S J, Balogh A and Forsyth R J 1995 *Journal of Geophysical Research: Space Physics* **100** 19903–19910 ISSN 2156-2202 URL <http://dx.doi.org/10.1029/95JA01123>
- [27] Moldwin M B, Ford S, Lepping R, Slavin J and Szabo A 2000 *Geophysical Research Letters* **27** 57–60 ISSN 1944-8007 URL <http://dx.doi.org/10.1029/1999GL010724>
- [28] Feng H Q, Wu D J and Chao J K 2007 *Journal of Geophysical Research: Space Physics* **112** ISSN 2156-2202 a02102 URL <http://dx.doi.org/10.1029/2006JA011962>
- [29] Cartwright M L and Moldwin M B 2008 *Journal of Geophysical Research: Space Physics* **113** ISSN 2156-2202 a09105 URL <http://dx.doi.org/10.1029/2008JA013389>
- [30] Feng H Q, Wu D J, Lin C C, Chao J K, Lee L C and Lyu L H 2008 *Journal of Geophysical Research: Space Physics* **113** ISSN 2156-2202 a12105 URL <http://dx.doi.org/10.1029/2008JA013103>
- [31] Cartwright M L and Moldwin M B 2010 *Journal of Geophysical Research: Space Physics* **115** ISSN 2156-2202 a08102 URL <http://dx.doi.org/10.1029/2009JA014271>
- [32] Feng H Q, Zhao G Q and Wang J M 2015 *Journal of Geophysical Research: Space Physics* **120** 10,175–10,184 ISSN 2169-9402 2015JA021643 URL <http://dx.doi.org/10.1002/2015JA021643>
- [33] Zank G P, le Roux J A, Webb G M, Dosch A and Khabarova O 2014 *The Astrophysical Journal* **797** 28 URL <http://stacks.iop.org/0004-637X/797/i=1/a=28>
- [34] le Roux J A, Webb G M, Zank G P and Khabarova O 2015 *Journal of Physics: Conference Series* **642** 012015 URL <http://stacks.iop.org/1742-6596/642/i=1/a=012015>
- [35] Sonnerup B U O and Teh W L 2008 *Journal of Geophysical Research: Space Physics* **113** ISSN 2156-2202 a05202 URL <http://dx.doi.org/10.1029/2007JA012718>
- [36] Hau L N and Sonnerup B U O 1999 *Journal of Geophysical Research: Space Physics* **104** 6899–6917 ISSN

- 2156-2202 URL <http://dx.doi.org/10.1029/1999JA900002>
- [37] Hu Q and Sonnerup B U O 2000 *Geophysical Research Letters* **27** 1443–1446 ISSN 1944-8007 URL <http://dx.doi.org/10.1029/1999GL010751>
- [38] deHoffmann F and Teller E 1950 *Phys. Rev.* **80**(4) 692–703 URL <http://link.aps.org/doi/10.1103/PhysRev.80.692>
- [39] Sonnerup B U O, Papamastorakis I, Paschmann G and Lühr H 1987 *Journal of Geophysical Research: Space Physics* **92** 12137–12159 ISSN 2156-2202 URL <http://dx.doi.org/10.1029/JA092iA11p12137>
- [40] Khrabrov A V and Sonnerup B U O 1998 *Journal of Geophysical Research: Space Physics* **103** 6641–6651 ISSN 2156-2202 URL <http://dx.doi.org/10.1029/97JA03731>
- [41] Trenchi L, Bruno R, D'Amicis R, Marcucci M F and Telloni D 2013 *Annales Geophysicae* **31** 1333–1341
- [42] Zank G P, Hunana P, Mostafavi P, Le Roux J A, Li G, Webb G M, Khabarova O, Cummings A, Stone E and Decker R 2015 *The Astrophysical Journal* **814** 137